HHS Public Access
Author manuscript
Sci Signal. Author manuscript; available in PMC 2020 December 03.

Published in final edited form as:
Sci Signal. ; 12(610): . doi:10.1126/scisignal.aax2057.

Biased M_1 receptor–positive allosteric modulators reveal role of phospholipase D in M_1-dependent rodent cortical plasticity

Sean P. Moran[1,2,3], **Zixiu Xiang**[2,3], **Catherine A. Doyle**[3], **James Maksymetz**[2,3], **Xiaohui Lv**[3], **Sehr Faltin**[3], **Nicole M. Fisher**[2,3], **Colleen M. Niswender**[2,3,4], **Jerri M. Rook**[1,2,3], **Craig W. Lindsley**[2,3,5], **P. Jeffrey Conn**[1,2,3,4,*]

[1]Vanderbilt Brain Institute, Vanderbilt University, Nashville, TN 37232, USA.

[2]Department of Pharmacology, Vanderbilt University, Nashville, TN 37232, USA.

[3]Vanderbilt Center for Neuroscience Drug Discovery, Vanderbilt University, Nashville, TN 37232, USA.

[4]Vanderbilt Kennedy Center, Vanderbilt University Medical Center, Nashville, TN 37240, USA.

[5]Department of Chemistry, Vanderbilt University, Nashville, TN 37232, USA.

Abstract

Highly selective, positive allosteric modulators (PAMs) of the M_1 subtype of muscarinic acetylcholine receptor have emerged as an exciting new approach to potentially improve cognitive function in patients suffering from Alzheimer's disease and schizophrenia. Discovery programs have produced a structurally diverse range of M_1 receptor PAMs with distinct pharmacological properties, including different extents of agonist activity and differences in signal bias. This includes biased M_1 receptor PAMs that can potentiate coupling of the receptor to activation of phospholipase C (PLC) but not phospholipase D (PLD). However, little is known about the role of PLD in M_1 receptor signaling in native systems, and it is not clear whether biased M_1 PAMs display differences in modulating M_1-mediated responses in native tissue. Using PLD inhibitors and PLD knockout mice, we showed that PLD was necessary for the induction of M_1-dependent long-term depression (LTD) in the prefrontal cortex (PFC). Furthermore, biased M_1 PAMs that did not couple to PLD not only failed to potentiate orthosteric agonist–induced LTD but also blocked M_1-dependent LTD in the PFC. In contrast, biased and nonbiased M_1 PAMs acted similarly in potentiating M_1-dependent electrophysiological responses that were PLD independent. These findings demonstrate that PLD plays a critical role in the ability of M_1 PAMs to modulate certain central nervous system (CNS) functions and that biased M_1 PAMs function differently in brain regions implicated in cognition.

[*]Corresponding author. jeff.conn@vanderbilt.edu.

Author contributions: S.P.M., Z.X., C.A.D., C.M.N., C.W.L., and P.J.C. designed experiments. S.P.M., Z.X., C.A.D., J.M., X.L., S.F., N.M.F., and J.M.R. performed experiments. S.P.M. and P.J.C. wrote the manuscript with input from all of the authors.

Competing interests: P.J.C., C.W.L., and C.M.N. are inventors on patents (AU2012328476; EP2770997; CA2853826; US9,586,964; and US8,772,509) that protect different classes of muscarinic acetylcholine receptor allosteric modulators. All other authors declare that they have no competing interests.

Data and materials availability: All data needed to evaluate the conclusions in the paper are present in the paper or the Supplementary Materials.

INTRODUCTION

The M_1 muscarinic acetylcholine receptor (mAChR) has attracted intense interest as a promising therapeutic target for the treatment of the cognitive disruptions in schizophrenia and Alzheimer's disease (AD). The M_1 receptor is highly expressed across many forebrain regions implicated in the pathophysiology of schizophrenia and AD, including the cortex, striatum, and hippocampus (1, 2). Dysregulation of the M_1 receptor has been reported within a subset of patients suffering from schizophrenia, which was illustrated by a marked reduction in M_1 receptor abundance in pyramidal neurons in cortical regions highly implicated in complex behaviors, such as cognition and working memory (3, 4). Furthermore, cholinesterase inhibitors, which increase overall acetylcholine (ACh) amounts by preventing the breakdown of ACh, provide some efficacy in patients with AD; however, dose-limiting adverse effects typically occur with disease progression. Therefore, selectively enhancing M_1 receptor signaling may provide a potential therapeutic approach for the treatment of the cognitive deficits associated with AD and schizophrenia.

Several orthosteric mAChR agonists, including the nonselective mAChR partial agonist xanomeline (5), have entered clinical trials as potential cognition-enhancing agents. Unfortunately, xanomeline failed to meet cognition enhancement end points, a result attributed to dose-limiting, nonselective cholinergic agonist adverse effects hypothesized to be mediated by the activation of peripheral M_2 and M_3 receptors (6–9). To increase selectivity for the M_1 receptor and therefore minimize nonselective adverse effects, multiple research efforts shifted to developing compounds that act through allosteric sites on mAChRs, which are structurally distinct from the orthosteric binding site and may be less highly conserved among receptor subtypes. To date, we and others have identified highly subtype-selective positive allosteric modulators (PAMs) of the M_1 receptor that avoid activation of other mAChR subtypes (10–12). Furthermore, M_1 receptor PAMs have shown robust efficacy in enhancing cognition and rescuing cognitive deficits in preclinical animal models relevant for AD and schizophrenia (13–18).

Although these preclinical findings are extremely promising for the potential of M_1 receptor PAMs to reverse cognitive deficits in patients, these PAMs can display a diverse range of pharmacological properties, some of which are potentially detrimental to in vivo efficacy. Previously, we found that the presence of allosteric agonist activity in M_1 receptor PAMs can limit in vivo efficacy and increase adverse effect liability (13, 14, 19, 20). Thus, minimalizing agonist activity could maximize the therapeutic window of M_1 receptor PAMs (13, 19–21). These previous studies demonstrate that a complete understanding of the different pharmacological properties of structurally distinct M_1 receptor PAMs is essential to fully evaluate clinical candidates and maximize their therapeutic potential.

In addition to displaying differences in allosteric agonist versus pure PAM activity, M_1 receptor PAMs can also differ in their ability to confer bias to M_1 receptor signaling. Signal bias is the phenomenon by which different G protein–coupled receptor (GPCR) ligands induce distinct active receptor-complex states that are biased toward specific signaling pathways (22). For example, characterization of a broad range of structurally diverse M_1 receptor PAMs revealed that some potentiate receptor signaling through the canonical phospholipase C (PLC) pathway but do not potentiate M_1 receptor–mediated activation of another phospholipase, phospholipase D (PLD) (23). PLD is a widely expressed enzyme that hydrolyzes the major plasma membrane phospholipid phosphatidylcholine into the signaling molecules phosphatidic acid (PA) and choline (24). PLD can be activated by various receptors, including the M_1 receptor (25, 26). Although there are six distinct mammalian isoforms of PLD, only PLD_1 and PLD_2 have well-established enzymatic activity within the central nervous system (CNS) (24, 27). However, little is known about the roles of PLD in regulating brain function, and the potential roles of PLD in M_1 receptor–dependent signaling have not been explored. Thus, it is unclear whether M_1 receptor PAMs that do not activate coupling of the receptor to PLD in cell lines will display functional differences in regulating M_1 signaling in the CNS relative to nonbiased M_1 receptor PAMs. For other GPCRs, signal bias provides the exciting potential advantage of selectively activating or potentiating therapeutically relevant pathways while minimizing activation of pathways responsible for adverse effects (11, 28, 29). Therefore, a better understanding of these signaling mechanisms is essential for the development of M_1 receptor PAMs as potential therapeutics for the treatment of prevalent cognitive disorders.

Here, we report that PLD activity is necessary for a form of M_1 receptor–dependent long-term depression (LTD) in the prefrontal cortex (PFC), which was previously implicated in the potential therapeutic response to M_1 receptor PAMs (14, 30, 31). Furthermore, biased M_1 PAMs that do not potentiate M_1 receptor coupling to PLD not only failed to potentiate this form of LTD but actively inhibited M_1 receptor–dependent LTD (M_1-LTD) at this synapse. In contrast, biased and nonbiased M_1 receptor PAMs functioned similarly in their ability to potentiate M_1 receptor–dependent responses in the CNS that we found to be PLD independent. Together, these studies reveal that PLD is a critical downstream signaling node for this M_1-LTD in the PFC and demonstrate that biased M_1 receptor PAMs can have fundamentally different effects, relative to those of nonbiased M_1 receptor PAMs, in regulating specific aspects of CNS function.

RESULTS

M_1 receptor activation leads to PLD activity in hM_1-CHO cells

M_1 receptor activation leads to an increase in PLD activity (25, 26), but it is not known whether this reflects activation of PLD_1, PLD_2, or both isoforms. Therefore, we set out to characterize the relative contributions of these two distinct PLD isoforms downstream of selective activation of M_1 in Chinese hamster ovary (CHO) cells stably expressing the M_1 receptor. Whereas direct measurement of the PLD product PA is challenging because of its rapid conversion into other lipids, such as diacylglycerol and lysophosphatidic acid, in the presence of a primary alcohol, such as 1-butanol, PLD generates the stable product phosphatidylbutanol (pButanol), which cannot be metabolized, therefore enabling quantification of intracellular PLD activity (24, 32, 33). Consistent with previous findings (23), the cholinergic orthosteric agonist carbachol (CCh) induced an increase in pButanol accumulation, which was blocked by the selective M_1 receptor antagonist VU0255035 (Fig. 1A) (34). Furthermore, the $PLD_{1,2}$ inhibitor ML299 (35) blocked M_1-mediated pButanol production, thereby supporting the suggestion that PLD was responsible for the generation of pButanol. Using more modern PLD_1 (VU0359595) (36) and PLD_2 (VU0364739) (37) isoform-selective inhibitors, we found that pharmacological inhibition of PLD_1, but not PLD_2, blocked the M_1-dependent activation of PLD in this in vitro assay (Fig. 1A). These data suggest that in this cell-based assay, M_1-dependent activation of PLD primarily occurs through PLD_1, not PLD_2.

Although we have previously characterized M_1 receptor PAMs that couple to PLC but not PLD (23), these early biased PAMs suffer from low potency and aqueous solubility. Therefore, we set out to develop additional M_1 receptor PAMs that potentiate M_1 receptor coupling to PLC but do not potentiate coupling to PLD. Previously, we reported that the M_1 receptor PAMs VU0453595 [half-maximal effective concentration (EC_{50}) = 2140 ± 440 nM], VU0405652 (EC_{50} = 2580 ± 440 nM), and VU0405645 (EC_{50} = 340 ± 30 nM) are potent M_1 receptor PAMs with respect to their ability to potentiate Ca^{2+} mobilization in CHO cells stably expressing the M_1 receptor (Fig. 1, B and C) (30, 38). We now report that unlike the prototypical M_1 receptor PAM VU0453595, both VU0405652 and VU0405645 failed to potentiate the CCh-dependent activation of PLD in this in vitro assay (Fig. 1D). These findings demonstrate that VU0405652 and VU0405645, but not VU0453595, are biased M_1 receptor PAMs in that they do not potentiate M_1 receptor coupling to PLD.

PLD_1, but not PLD_2, is required for M_1 receptor–mediated LTD in the mPFC

From the cell-based assay, we know that M_1 receptor activation can increase PLD activity; however, little is known about whether PLD is necessary for M_1-dependent responses in native neuronal tissue. Therefore, we set out to characterize the role of PLD in mediating established responses to M_1 receptor activation in CNS preparations. One response to M_1 receptor activation that may be relevant to some aspects of cognitive function is the induction of LTD of excitatory synaptic transmission in the medial PFC (mPFC) (13, 14, 19, 30, 31, 39). We assessed the role of PLD in inducing LTD in the mPFC by measuring changes in layer V field excitatory postsynaptic potentials (fEPSPs) evoked by electrical stimulation of afferents in layer II/III of the mPFC (Fig. 2A). Consistent with previous findings (13, 14, 30, 39), a maximal concentration of CCh induced robust LTD of the fEPSP slope at this synapse (Fig. 2B). To test whether PLD was required for CCh-induced LTD, we bath-applied the $PLD_{1,2}$ inhibitor ML299 for 10 min before and throughout CCh application, which resulted in a complete loss of CCh-induced LTD (Fig. 2C). Using selective inhibitors for each PLD isoform, we found that pharmacological inhibition of PLD_1 with VU0359595 fully blocked CCh-induced LTD (Fig. 2D). Congruent with the cell-based assay findings, inhibition of PLD_2 with VU0364739 had no effect on CCh-induced LTD at this synapse (Fig. 2E). Quantification of fEPSP slopes 46 to 50 min after drug washout indicated that ML299 and VU0359595 statistically significantly attenuated CCh-induced LTD, whereas inhibition of PLD_2 with VU0364739 had no significant effect (Fig. 2F).

To confirm these pharmacological results, we obtained PLD_1 knockout (KO) mice and subsequently confirmed that PLD_1 abundance was reduced in cortical tissue compared to that in the cortical tissue of wild-type littermate controls (fig. S1). Consistent with our pharmacological findings, CCh induced a robust LTD in slices obtained from littermate controls but not from PLD_1 KO mice (Fig. 2, G and H). Furthermore, the ability of a selective agonist of group II metabotropic glutamate receptors (LY379268) to induce LTD was intact in the PLD_1 KO mice and not statistically significantly different from that in littermate controls (Fig. 2, I and J). This form of LTD has been previously characterized in detail and is mechanistically distinct from M_1-dependent LTD in the mPFC (40–42). Furthermore, input-output curves generated by comparing fiber volley slope to fEPSP slope (fig. S2A) did not appear to differ between genotypes (fig. S2B). These data suggest that the loss of M_1-mediated LTD is not due to a general deficit in LTD in this brain region. Together, these data demonstrate a critical role of PLD, specifically PLD_1, in this form of cortical M_1-LTD.

Biased M_1 receptor PAMs fail to potentiate M_1-LTD in the mPFC

We next tested the hypothesis that biased and nonbiased M_1 receptor PAMs would display functional differences in their ability to potentiate this PLD-dependent, CCh-induced LTD of layer V fEPSPs electrically evoked in layer II/III in the mPFC. As previously shown, a submaximal concentration of CCh (10 μM) did not induce LTD at this synapse (Fig. 3A) (13, 19, 30). Similar to previous findings, bath application of the nonbiased M_1 receptor PAM VU0453595 for 10 min before and during CCh application leads to a robust LTD (Fig. 3B). Consistent with a role for PLD in inducing M_1-LTD, neither of the biased M_1 receptor PAMs VU0405652 (Fig. 3C) or VU0405645 (Fig. 3D) potentiated the LTD response to a submaximal concentration of CCh. Quantification of fEPSP slopes after drug washout indicated a statistically significant depression of fEPSP slope compared to baseline with the M_1 receptor PAM VU0453595 but not with VU0405652 or VU0405645 (Fig. 3E).

Theoretically, M_1 receptor PAMs that confer this form of biased M_1 receptor signaling would stabilize a conformation of M_1 receptor that favors activation of signaling by PLC but not PLD (43–46). On the basis of this, if these PAMs confer true bias to M_1 receptor signaling, they should inhibit PLD-mediated responses. Thus, we tested the hypothesis that PAMs that bias M_1 receptor signaling away from PLD would therefore block the LTD normally induced by a maximal concentration of CCh (Fig. 3F). In agreement with our hypothesis, both VU0405645 (Fig. 3F) and VU0405652 (Fig. 3, G and H) blocked CCh-induced LTD (Fig. 3H). Together, these findings demonstrate a role for PLD in this cortical M_1-LTD and that biased M_1 receptor PAMs not only fail to potentiate LTD in response to a submaximal concentration of CCh but also actively block LTD in response to a maximal concentration of CCh.

PLD is not necessary for the M_1 receptor–dependent increase in layer V sEPSCs in the mPFC

In light of these findings, we next set out to determine whether PLD was important in other M_1-dependent functions in the CNS. Previously, we reported that M_1 receptor activation increases the frequency of spontaneous excitatory postsynaptic currents (sEPSCs) in mPFC layer V pyramidal neurons (15, 19, 30). Consistent with these previous findings, bath application of a maximal concentration of CCh induced a robust increase in sEPSC frequency in layer V pyramidal neurons (Fig. 4A). In contrast to M_1-dependent LTD, the effect of CCh on sEPSCs was unchanged by pretreatment and co-application of the dual PLD inhibitor ML299 (Fig. 4B). Quantification of the peak CCh effect on sEPSC frequency indicated no statistically significant difference between CCh alone and CCh in the presence of ML299 (Fig. 4C). These data suggest that PLD is not necessary for this M_1-dependent increase of sEPSC frequency in mPFC layer V pyramidal neurons.

Next, we sought to compare the two biased M_1 receptor PAMs, VU0405652 and VU0405645, with our prototypical M_1 receptor PAM, VU0453595, in terms of their ability to potentiate a submaximal concentration of CCh-induced increases in mPFC layer V pyramidal neuron sEPSC frequency. As expected, bath application of a submaximal concentration of CCh did not induce a statistically significant change in sEPSC frequency (Fig. 4D). Similar to the M_1 receptor PAM BQCA (benzyl quinolone carboxylic acid) (15), the nonbiased M_1 receptor PAM VU0453595 induced a robust potentiation of the effect of a submaximal concentration of CCh on sEPSC frequency (Fig. 4E), and this effect was attenuated by pharmacological inhibition of PLC with the PLC inhibitor U73122 (fig. S3, A to D). Consistent with the studies with PLD inhibitors, both VU0405652 (Fig. 4F) and VU0405645 (Fig. 4G) potentiated agonist-induced increases in sEPSC frequency. Quantification of the peak effect on sEPSC frequency indicated a statistically significant difference between CCh alone and CCh with any of the three M_1 receptor PAMs (Fig. 4H). Therefore, these data suggest that both biased and nonbiased M_1 receptor PAMs function similarly in their ability to potentiate increases in mPFC layer V pyramidal neuron sEPSC frequency in response to a submaximal concentration of agonist (Fig. 4I).

PLD is not necessary for the effects of the M_1 receptor on the excitability of striatal SPNs

The M_1 receptor is also highly abundant in the striatum (47), and we previously showed that M_1 receptor activation in spiny projection neurons (SPNs) in the dorsal lateral striatum leads to a robust increase in SPN excitability that can be blocked by a selective M_1 receptor antagonist (48, 49). Therefore, we set out to determine whether PLD was required for this M_1-dependent response. As expected, bath application of CCh induced a robust increase in dorsal lateral striatum SPN excitability (Fig. 5A). In the presence of the $PLD_{1,2}$ inhibitor ML299, CCh still induced a marked increase in SPN excitability compared to baseline (Fig. 5B). Quantification of the CCh-induced increase in SPN excitability showed no statistically significant difference between the change in number of spikes per pulse between the control [dimethyl sulfoxide (DMSO)] and ML299 groups (Fig. 5C). Therefore, similar to the sEPSC findings, PLD is not necessary for M_1-dependent increases in dorsal lateral SPN excitability.

The finding that PLD is not involved in M_1 receptor–mediated regulation of SPN excitability suggests that biased M_1 receptor PAMs that selectively potentiate coupling to PLC and do not potentiate PLD activity would function similarly to nonbiased M_1 receptor PAMs in their ability to potentiate responses to a low concentration of CCh on SPN excitability. In agreement with our previous findings (49), a submaximal concentration of CCh induced a minimal increase in SPN excitability (Fig. 5D) that was robustly potentiated by the prototypical M_1 receptor PAM VU0453595 (Fig. 5E). As expected, both VU0405652 (Fig. 5F) and VU0405645 (Fig. 5G) potentiated an increase in SPN excitability in response to a submaximal concentration of CCh. The maximal increase in the number of spike discharges during agonist application was statistically significantly higher in the presence of each of the three M_1 receptor PAMs compared to the DMSO control condition (Fig. 5, H and I).

Furthermore, in these studies, the concentration of VU0453595 used induced a more robust effect than did the same concentrations of VU0405652 or VU0405645. However, on the basis of the current results, it is unclear whether the concentrations used provide a maximal effect on SPN excitability. Thus, it is not clear whether this apparent difference represents differences in the relative efficacies of the different PAMs or differences in slice penetration and their final concentrations at the M_1 receptor. However, these results demonstrate that biased and nonbiased M_1 receptor PAMs function similarly in their ability to potentiate M_1 receptor–dependent regulation of SPN excitability and other CNS responses that are PLD independent.

DISCUSSION

A large body of clinical and preclinical research suggests that enhancing mAChR signaling can be efficacious in the treatment of the cognitive symptoms associated with AD and schizophrenia (7, 8, 50, 51). Although multiple mAChR subtypes are involved in the regulation of cognitive function, most preclinical studies point to a dominant role of the M_1 receptor and suggest that its selective modulation may provide a therapeutic potential for the treatment of these devastating cognitive symptoms (14, 15, 17–19, 30, 52–58). However, M_1 receptors regulate CNS function by actions on multiple signaling pathways, and M_1 receptor PAMs can display a diverse range of pharmacological properties, including signal bias. At present, little is known about the specific signaling pathways involved in the different physiological effects of M_1 receptor activation or how signal bias can affect the PAM-mediated modulation of M_1 receptor actions in identified brain circuits. The present studies improve our understanding of at least one mechanism by which M_1 receptor activation leads to plasticity changes within a key cortical structure in the CNS. Specifically, we found that a previously described M_1-dependent LTD in the cortex was dependent on the activation of PLD. Furthermore, we identified M_1 receptor PAMs that selectively enhanced M_1 receptor coupling to PLC but not PLD and found that these biased M_1 receptor PAMs failed to potentiate this form of M_1-dependent LTD. Last, these biased M_1 receptor PAMs actively blocked the ability of mAChR agonists to induce this PLD-dependent LTD, consistent with the hypothesis that these PAMs stabilize a conformation of the M_1 receptor that favors activation of PLC over PLD and thereby bias M_1 receptor signaling in favor of PLC-mediated responses. Furthermore, not all M_1-dependent responses were PLD dependent, and biased M_1 receptor PAMs functioned similarly to nonbiased M_1 PAMs in cases where M_1 receptor signaling was PLD independent.

Although the ability of the M_1 receptor and other GPCRs to activate PLD is well established (59), little is known about the physiological roles of PLD in regulating CNS function. This has largely been due to the lack of selective inhibitors and other tools that enable systematic studies of PLD-mediated responses. However, the discovery of the highly selective PLD inhibitors used here (35–37), together with the generation of PLD KO mice and the biased M_1 receptor PAMs reported in the present studies, provided an unprecedented opportunity to determine the roles of PLD in mediating specific responses to M_1 receptor activation. With the availability of these new tools, these studies provide an example of a specific physiological role of PLD in mediating a response to GPCR activation in the CNS and reveal a previously uncharacterized role for PLD in the induction of major form of synaptic plasticity in an identified brain circuit. Furthermore, these PLD inhibitors include selective inhibitors of PLD_1 and PLD_2, the major isoforms of PLD expressed in the CNS. Experiments with these isoform-selective inhibitors, together with PLD_1 KO mice, revealed a critical role for PLD_1 as the PLD isoform involved in mediating this response to M_1 receptor activation.

M_1-dependent LTD in the mPFC has been extensively studied and has been postulated to play a critical role in regulating specific inputs to the mPFC from the hippocampus and other extrinsic afferents (60, 61). Cholinergic regulation of these inputs is thought to be important for the regulation of multiple aspects of mPFC function, and previous studies suggest that M_1 receptor expression and signaling in the mPFC can be impaired in some pathological states that could be relevant for schizophrenia and AD (3, 14, 30, 62–68). However, very few studies have focused on understanding the cellular mechanisms underlying M_1-dependent LTD in the PFC. Although the current studies identify PLD_1 as being critically important in M_1-dependent cortical synaptic plasticity, the detailed molecular mechanism by which the M_1 receptor signals through PLD to induce synaptic plasticity changes in the cortex remains unknown. Rigorous molecular and biochemical studies to elucidate this signaling pathway are necessary to fully understand the signaling cascade responsible for M_1-dependent LTD.

The finding that PLD_1 is important for this form of synaptic plasticity, coupled with the finding that biased and nonbiased M_1 receptor PAMs have functionally distinct effects on this response, raises the possibility that different PAMs could have unique profiles in regulating cognitive function or other in vivo responses. It is possible that biased versus nonbiased M_1 receptor PAMs could induce markedly different effects on specific behavioral responses, as is the case for biased and nonbiased PAMs of the $mGlu_5$ subtype of metabotropic glutamate (mGlu) receptors (69, 70). Unfortunately, the currently available biased M_1 receptor PAMs used in the present studies do not have appropriate properties to enable their use in behavioral studies in vivo (table S1). However, in future studies, it may be possible to optimize biased M_1 receptor PAMs that can be used to systematically evaluate the roles of PLD in specific behavioral responses that are dependent on M_1 receptor activation. Extensive medicinal chemistry efforts are needed to develop biased M_1 receptor PAMs that have favorable physical and pharmacokinetic properties suitable for systemic administration with high CNS penetrance to test whether systemically administered biased M_1 PAMs display functional differences in their ability to reverse the cognitive deficits in preclinical animals relevant for AD and schizophrenia.

Last, in future studies, it will also be important to develop an understanding of the precise molecular mechanisms involved in conferring bias for some M_1 receptor PAMs. Whereas there are multiple examples of allosteric modulators of GPCRs that induce biased signaling, little is known about the structural basis of biased versus nonbiased signaling. Previous studies revealed multiple allosteric binding sites for some GPCRs, which could contribute to different responses to distinct classes of allosteric modulators (71–73). However, other studies suggest that differences in M_1 receptor PAM functionality may not be due to binding to different allosteric binding pockets but that binding of PAMs to a single allosteric site may stabilize different receptor conformational states (74, 75). Understanding how allosteric modulators of GPCRs induce their effects will help facilitate the rational design of the next generation of PAMs and negative allosteric modulators.

MATERIALS AND METHODS

Cell lines and Ca^{2+} mobilization assay

Briefly, M_1-CHO cells were plated in black-walled, clear-bottomed 384-well plates (Greiner Bio-One) the day before assay. On the next day, the cells were washed with assay buffer (Hank's balanced salt solution, 20 mM Hepes, 4.16 mM sodium bicarbonate, and 2.5 mM probenecid) and immediately incubated with 20 µl of 1.15 µM fluo-4-acetomethoxyester (Fluo-4 AM) dye solution prepared in assay buffer for 45 min at 37°C. The M_1 PAMs were serially diluted (1:3) in DMSO for 10-point concentration−response curves and further diluted in assay buffer using Echo liquid handler (Labcyte). After the dye was removed, the cells were washed with assay buffer and Ca^{2+} flux was immediately measured using the Functional Drug Screening System (FDSS7000, Hamamatsu Photonics). The serially diluted compounds or DMSO (vehicle) was added to the cells for 2.5 min; then, an EC_{20} concentration of ACh was added and incubated for 2 min. An EC_{max} concentration of ACh was also added to cells that were incubated with DMSO to ensure the EC_{20} calcium response. To determine the potency and efficacy of the agonist and PAM, data were analyzed to generate a concentration-response curve using a four-point logistic equation in GraphPad Prism 5.0 (GraphPad Software Inc.).

PLD activity assay

Methods were adapted from a previously published procedure (59). Briefly, CHO cells stably transfected with plasmid encoding the human mAChR were cultured in growth medium consisting of Ham's F-12 Nutrient Mix (Thermo Fisher Scientific, #11765), 10% fetal bovine serum (FBS), 20 mM Hepes, 1× antibiotic/antimycotic, and 500 µM G418. The cells were then plated on six-well plates at a density of about 0.7×10^6 cells per 2 ml per well. Plating medium consisted of growth medium without FBS or G418. The following day, plating medium was removed by aspiration, and labeling medium was prepared by adding [^{3}H]palmitic acid (5 µCi/µl) supplemented with phosphor-ethanolamine (2.08 µg/µl) (PE stock; 25 mg/ml in $CHCl_3$) to serum-free medium supplemented with bovine serum albumin. Each well contained 1 ml of medium with 10 to 30 µCi of [^{3}H]palmitic acid. Labeling was allowed to occur in a 37°C incubator overnight. The next morning, the plating medium was carefully removed by aspiration and the cells were treated for 5 min with DMSO or the appropriate M_1 PAM (no agonist) and then for 30 min in the presence or absence (negative control) of 0.3% 1-butanol and the cholinergic agonist CCh in serum-free assay medium (1 ml of medium per well), and the plates were incubated at 37°C. ^{3}H labeling efficiency was measured by subtracting the postlabeling medium from the prelabeling medium. All pharmacological agent stocks were used at 500- or 1000-fold higher than the final concentration. Immediately after the incubation, 600 µl of ice-cold, acidified methanol (1:1 ratio of 0.1 N HCl to methanol) was added and the cells were scraped off with a cell scraper and transferred to a 1.5-ml Eppendorf tube. Room temperature $CHCl_3$ (300 µl) was then added, and the sample was then vortexed vigorously for about 20 s. The samples were then spun at 16,000*g* for 5 min to separate phases. The bottom lipid phase was removed carefully to ensure that no other phases were carried over and was transferred to a new 1.5-ml Eppendorf tube. The samples were then dried under N_2 gas until all of the liquid was evaporated. The lipids were then resuspended in 25 µl of $CHCl_3$ and immediately spotted onto the thin-layer chromatography (TLC) plate (Sorbtech; catalog no. 2315126C). Nonradioactive lipid standards such as pButanol and PA were also spotted on the TLC plate. The TLC tank was prepared by placing chromatography paper [7 inches (height) by 22.5 inches (width)] so that it covered about 75% of the tank's height. The mobile phase was then added (10 $CHCl_3$:2 methanol:2 acetic acid:4 acetone:1 H_2O) and allowed to equilibrate for 1 hour before the TLC plate was added and run for 1.5 to 2 hours. The plate was then removed from the tank and allowed to completely dry before imaging using autoradiography film in conjunction with an intensifying screen (BioMax TranScreen LE, Carestream Health) and placed in a −80°C freezer for 3 to 5 days. The film was then processed after exposure and quantified with ChemiDoc (Bio-Rad).

Animals

All animal studies were approved by the Vanderbilt University Medical Center Institutional Animal Care and Use Committee and were conducted in accordance with the National Institutes of Health (NIH) *Guide for the Care and Use of Laboratory Animals*. Six- to 10-week-old male and female C57BL6/J mice (The Jackson Laboratory) and both male and female PLD_1 KO mice (obtained from the trans-NIH Knockout Mouse Project Repository; www.komp.org) maintained on a C57BL6/J background were used in electrophysiology studies. Mice were group-housed at four to five per cage and maintained on a 12-hour light/12-hour dark cycle, and food and water were provided ad libitum.

In vivo pharmacokinetic analysis

VU0405652 and VU0405645 compounds were formulated as 10% Tween 80 in sterile water at a concentration of 3 mg/ml and administered intraperitoneally to male C57BL6/J mice and dosed at 30 mg/kg. Mouse blood (cardiac puncture) and brains were collected at 15 and 30 min. Animals were euthanized and decapitated, and the brains were removed, thoroughly washed in ice-cold (4°C) phosphate-buffered saline, and immediately frozen on dry ice. Brain samples were processed, and the concentrations of compound were determined by electrospray ionization on an AB SCIEX API 4000 triple-quadrupole instrument that was coupled with Shimadzu LC-10AD pumps and a Leap Technologies CTC PAL auto-sampler. All data were analyzed with AB SCIEX Analyst 1.5.1 software. Compound exposures, in the form of area under the curve, were calculated by the trapezoidal method with PRISM software (GraphPad).

Whole-cell electrophysiology

Mice were anesthetized with isoflurane and then transcardially perfused with ice-cold cutting solution (230 mM sucrose, 2.5 mM KCl, 8 mM $MgSO_4$, 0.5 mM $CaCl_2$, 1.25 mM NaH_2PO_4, 10 mM D-glucose, and 26 mM $NaHCO_3$), and the brains were removed and then submerged in ice-cold cutting solution. Coronal slices containing either dorsal striatum or prelimbic PFC were cut at a thickness of 250 or 300 µm, respectively, and were transferred to a holding chamber containing *N*-methyl-D-glucamine (NMDG)–Hepes recovery solution [93 mM NMDG, 2.5 mM KCl, 1.2 mM NaH_2PO_4, 30 mM $NaHCO_3$, 20 mM Hepes, 25 mM

D-glucose, 5 mM sodium ascorbate, 2 mM thiourea, 3 mM sodium pyruvate, 10 mM $MgSO_4$, 0.5 mM $CaCl_2$, and 12 mM *N*-acetyl-L-cysteine (pH 7.35), <310 mOsm] for 8 to 10 min at 32°C. Slices were then transferred to a room temperature holding chamber for 1 hour containing artificial cerebrospinal fluid (ACSF) (126 mM NaCl, 1.25 mM NaH_2PO_4, 2.5 mM KCl, 10 mM D-glucose, 26 mM $NaHCO_3$, 2 mM $CaCl_2$, and 1 mM $MgSO_4$) supplemented with 600 μM sodium ascorbate for slice viability. All buffers were continuously bubbled with 95% O_2/5% CO_2. Subsequently, slices were transferred to a 30° to 31°C submersion recording chamber (Warner Instruments), where they were perfused with ACSF at a rate of 2 ml/min. Recording pipettes were constructed from thin-walled borosilicate capillary glass tubing (inner diameter, 1.17 mm; outer diameter, 1.50 mm; Warner Instruments), pulled with a horizontal pipette puller (P-97 Sutter Instrument Co.) to a resistance of 4 to 6 megaohms when filled with potassium-based internal solution: 125 mM potassium gluconate, 4 mM NaCl, 10 mM Hepes, 4 mM magnesium adenosine 5′-triphosphate (MgATP), 0.3 mM sodium guanosine 5′-triphosphate (NaGTP), and 10 mM tris-phosphocreatine. For the PFC recordings, pyramidal neurons were visualized on the basis of morphology with a 40× water-immersion lens with oblique illumination coupled with an Olympus BX50WI upright microscope (Olympus). After a stable gigaohm seal was formed, light suction was applied to break through the cell membrane and achieve whole-cell access. The access resistance was checked at the beginning and the end of each experiment, and neurons with an access resistance of >30 megaohms were not used for analysis. Pyramidal neurons were further identified by their regular spiking pattern after depolarizing current injections induced by a series of 500-ms current steps (−150 to +100 pA) in +25-pA increments performed in current clamp mode. sEPSCs were recorded at a holding potential of −70 mV [the reversal potential for γ-aminobutyric acid type A ($GABA_A$) channels], and the junction potential was not compensated. The voltage clamp signal was low pass–filtered at 5 kHz and digitized at 10 kHz with a Digidata 1322A, acquired with an Axon MultiClamp 700B (Molecular Devices), and controlled by pCLAMP 9.2 and Clampex 10.6.2 running on a Dell PC. After a stable baseline was recorded for 5 to 10 min, test compounds were diluted to the appropriate concentrations in DMSO (<0.1% final) in ACSF and applied to the bath using a peristaltic pump perfusion system. Cumulative probability plots of interevent intervals (IEIs) were constructed using 2-min episodes of baseline and peak effect during drug application. To determine whether the potentiation of sEPSC frequency by M_1 receptor PAMs was dependent on PLC, we included 1 μM U73122 (Tocris Bioscience) or DMSO in the internal solution and constantly perfused 10 μM U73122 or DMSO (0.2%) ACSF throughout the entire experiment. All sEPSC analyses were performed with MiniAnalysis (Synaptosoft Inc.) or Clampfit 10.2 (Molecular Devices). For striatal SPN recordings, the change in excitability of SPN was assessed in current clamp mode by monitoring the change in the number of spike discharges in response to a near rheobase depolarization current step (1.0 s). The access resistance was checked at the beginning and the end of each experiment, which was compensated using “bridge balance.” The change in spike number was calculated by averaging the number of spikes during the baseline subtracted from the peak drug effect (60 s). Offline data analysis to calculate changes in SPN excitability was performed with Clampfit 10.2 (Molecular Devices).

Extracellular field electrophysiology

Coronal slices (400 μm) containing the PFC were obtained as described earlier. Recording pipettes were constructed from thin-walled borosilicate capillary glass tubing (inner diameter, 1.17 mm; outer diameter, 1.50 mm; Warner Instruments), pulled with a horizontal pipette puller (P-97 Sutter Instrument Co.) to a resistance of 1 to 3 megaohms when filled with ACSF. fEPSPs were recorded from layer V of the prelimbic cortex and evoked electrically by a concentric bipolar stimulating electrode (200-μs duration, 0.05 Hz; interpulse interval of 50 ms) in the superficial layers II to III. Layer II/III was visualized with a Olympus BX50WI upright microscope (Olympus) according to the landmarks illustrated in the Allen Mouse Brain Atlas (76), and the recording electrode was placed laterally about 200 μm away from layer II/III into layer V so that the recording and stimulating electrodes were parallel to each other. Input-output curves were generated to determine the stimulus intensity that produced about 70% of the maximum fEPSP slope before each experiment, which was then used as the baseline stimulation. Data were digitized with a MultiClamp 700B using a sampling rate of 20,000 kHz and filtered at 0.5 kHz with a Digidata 1322A, pCLAMP 9.2, and Clampex 10.6.2 software (Molecular Devices) running on a Dell PC. All test compounds, with the exception of CCh (Tocris Bioscience), which was diluted in H_2O, were diluted to the appropriate concentrations in DMSO (<0.1% final) in ACSF and applied to the bath using a peristaltic pump perfusion system. Offline data analysis to calculate fEPSP slope was performed with Clampfit 10.2 (Molecular Devices).

Western blotting analysis of PLD_1

Total protein was extracted from the cortex of PLD_1 KO mice and littermate controls by homogenization in radioimmunoprecipitation assay buffer (Sigma) with protease inhibitors. After homogenization, samples were spun for 20 min at 15,000*g* at 4°C. The supernatant was kept, and protein concentration was determined using a bicinchoninic acid protein assay (Pierce). Protein (50 μg per sample) was electrophoretically resolved using a 4 to 20% SDS polyacrylamide gel and transferred onto a nitrocellulose membrane using iBlot 2 (Thermo Fisher Scientific). The membrane was blocked with Odyssey blocking buffer (LI-COR) for 1 hour at room temperature. Membranes were incubated overnight at 4°C with the following primary antibodies: rabbit anti-PLD_1 (1:500 dilution; Cell Signaling Technology, 3832) and mouse anti-tubulin (1:5000; Abcam, ab44928). Membranes were washed with TBST (25 mM tris, 150 mM NaCl, and 0.05% Tween 20) and incubated with fluorescently labeled secondary antibodies (goat anti-rabbit 800 and goat anti-mouse 680; 1:5000; LI-COR) for 1 hour at room temperature. Blots were washed again and imaged with a LI-COR Odyssey device.

Statistical analysis

Two-tailed Student's *t* tests and one-way analysis of variance (ANOVA) with Bonferroni post tests were used as appropriate. Changes in fEPSP slope before and during drug add (peak effect) were compared using a paired *t* test. For all statistical comparisons, the critical *P* value was considered to be 0.05. The numbers of animals to be used for each experiment outlined within the study were determined using a power calculation statistical analysis using the Power and Sample Size Calculation software program available at Vanderbilt University (Dupont and Plummer, PS Controlled Clinical Trials. 18:274 1997). Animal numbers are based on a power calculation using SEs from published studies and previous experience to detect >20% difference for each outlined experiment with an 80% power (α = 0.05, power = 80%, δ = 0.2, σ = 0.18).

Supplementary Material

Refer to Web version on PubMed Central for supplementary material.

Acknowledgments:

We thank the Dan Marino Foundation for support of the Clinical Neuroscience Scholars Program at Vanderbilt University. We thank W. Peng for excellent assistance in maintaining colonies and genotyping of transgenic mice.

Funding: This work was supported by NIH F31 MH114368 (S.P.M.), NIH T32 MH 64913 (S.P.M.), U01 MH087965 (P.J.C.), R01 MH062646 (P.J.C.), R01 MH073676 (P.J.C.), and R01 MH082867 (C.W.L.).

REFERENCES AND NOTES

1. Masters CL, Bateman R, Blennow K, Rowe CC, Sperling RA, Cummings JL, Alzheimer's disease. Nat. Rev. Dis. Primers 1, 15056 (2015). [PubMed: 27188934]
2. Lieberman JA, M. B, Psychotic disorders. N. Engl. J. Med 379, 270–280 (2018). [PubMed: 30021088]
3. Scarr E, Hopper S, Vos V, Seo MS, Everall IP, Aumann TD, Chana G, Dean B, Low levels of muscarinic M1 receptor-positive neurons in cortical layers III and V in Brodmann areas 9 and 17 from individuals with schizophrenia. J. Psychiatry Neurosci 43, 338–346 (2018). [PubMed: 30125244]
4. Euston DR, Gruber AJ, McNaughton BL, The role of medial prefrontal cortex in memory and decision making. Neuron 76, 1057–1070 (2012). [PubMed: 23259943]
5. Heinrich JN, Butera JA, Carrick T, Kramer A, Kowal D, Lock T, Marquis KL, Pausch MH, Popiolek M, Sun S-C, Tseng E, Uveges AJ, Mayer SC, Pharmacological comparison of muscarinic ligands: Historical versus more recent muscarinic M1-preferring receptor agonists. Eur. J. Pharmacol 605, 53–56 (2009). [PubMed: 19168056]
6. Bender AM, Jones CK, Lindsley CW, Classics in chemical neuroscience: Xanomeline. ACS Chem. Nerosci 8, 435–443 (2017).
7. Bodick NC, Offen WW, Levey AI, Cutler NR, Gauthier SG, Satlin A, Shannon HE, Tollefson GD, Rasmussen K, Bymaster FP, Hurley DJ, Potter WZ, Paul SM, Effects of xanomeline, a selective muscarinic receptor agonist, on cognitive function and behavioral symptoms in Alzheimer disease. Arch. Neurol 54, 465–473 (1997). [PubMed: 9109749]
8. Shekhar A, Potter WZ, Lightfoot J, Lienemann J, Dubé S, Mallinckrodt C, Bymaster FP, McKinzie DL, Felder CC, Selective muscarinic receptor agonist xanomeline as a novel treatment approach for schizophrenia. Am. J. Psychiatry 165, 1033–1039 (2008). [PubMed: 18593778]
9. Bymaster FP, Carter PA, Yamada M, Gomeza J, Wess J, Hamilton SE, Nathanson NM, McKinzie DL, Felder CC, Role of specific muscarinic receptor subtypes in cholinergic parasympathomimetic responses, in vivo phosphoinositide hydrolysis, and pilocarpine-induced seizure activity. Eur. J. Neurosci 17, 1403–1410 (2003). [PubMed: 12713643]
10. Yohn SE, Conn PJ, Positive allosteric modulation of M_1 and M_4 muscarinic receptors as potential therapeutic treatments for schizophrenia. Neuropharmacology 136, 438–448 (2018). [PubMed: 28893562]
11. Foster DJ, Conn JP, Allosteric modulation of GPCRs: New insights and potential utility for treatment of schizophrenia and other CNS disorders. Neuron 94, 431–446 (2017). [PubMed: 28472649]

12. Bock A, Schrage R, Mohr K, Allosteric modulators targeting CNS muscarinic receptors. Neuropharmacology 136, 427–437 (2017). [PubMed: 28935216]

13. Rook JM, Bertron JL, Cho HP, Garcia-Barrantes PM, Moran SP, Maksymetz JT, Nance KD, Dickerson JW, Remke DH, Chang S, Harp JM, Blobaum AL, Niswender CM, Jones CK, Stauffer SR, Conn PJ, Lindsley CW, A novel M1 PAM VU0486846 exerts efficacy in cognition models without displaying agonist activity or cholinergic toxicity. ACS Chem. Nerosci 9, 2274–2285 (2018).

14. Grannan MD, Mielnik CA, Moran SP, Gould RW, Ball J, Lu Z, Bubser M, Ramsey AJ, Abe M, Cho HP, Nance KD, Blobaum AL, Niswender CM, Conn PJ, Lindsley CW, Jones CK, Prefrontal cortex-mediated impairments in a genetic model of NMDA receptor hypofunction are reversed by the novel M1 PAM VU6004256. ACS Chem. Nerosci 7, 1706–1716 (2016).

15. Shirey JK, Brady AE, Jones PJ, Davis AA, Bridges TM, Kennedy JP, Jadhav SB, Menon UN, Xiang Z, Watson ML, Christian EP, Doherty JJ, Quirk MC, Snyder DH, Lah JJ, Levey AI, Nicolle MM, Lindsley CW, Conn PJ, A selective allosteric potentiator of the M_1 muscarinic acetylcholine receptor increases activity of medial prefrontal cortical neurons and restores impairments in reversal learning. J. Neurosci 29, 14271–14286 (2009). [PubMed: 19906975]

16. Choy KHC, Shackleford DM, Malone DT, Mistry SN, Patil RT, Scammells PJ, Langmead CJ, Pantelis C, Sexton PM, Lane JR, Christopoulos A, Positive allosteric modulation of the muscarinic M_1 receptor improves efficacy of antipsychotics in mouse glutamatergic deficit models of behavior. J. Pharmacol. Exp. Ther 359, 354–365 (2016). [PubMed: 27630144]

17. Uslaner JM, Eddins D, Puri V, Cannon CE, Sutcliffe J, Chew CS, Pearson M, Vivian JA, Chang RK, Ray WJ, Kuduk SD, Wittmann M, The muscarinic M1 receptor positive allosteric modulator PQCA improves cognitive measures in rat, cynomolgus macaque, and rhesus macaque. Psychopharmacology 225, 21–30 (2013). [PubMed: 22825578]

18. Lange HS, Cannon CE, Drott JT, Kuduk SD, Uslaner JM, The M_1 muscarinic positive allosteric modulator PQCA improves performance on translatable tests of memory and attention in rhesus monkeys. J. Pharmacol. Exp. Ther 355, 442–450 (2015). [PubMed: 26446308]

19. Moran SP, Dickerson JW, Cho HP, Xiang Z, Maksymetz J, Remke DH, Lv X, Doyle CA, Rajan DH, Niswender CM, Engers DW, Lindsley CW, Rook JM, Conn PJ, M_1-positive allosteric modulators lacking agonist activity provide the optimal profile for enhancing cognition. Neuropsychopharmacology 43, 1763–1771 (2018). [PubMed: 29581537]

20. Moran SP, Cho HP, Maksymetz J, Remke DH, Hanson RM, Niswender CM, Lindsley CW, Rook JM, Conn PJ, PF-06827443 displays robust allosteric agonist and positive allosteric modulator activity in high receptor reserve and native systems. ACS Chem. Nerosci 9, 2218–2224 (2018).

21. Rook JM, Abe M, Cho HP, Nance KD, Luscombe VB, Adams JJ, Dickerson JW, Remke DH, Garcia-Barrantes PM, Engers DW, Engers JL, Chang S, Foster JJ, Blobaum AL, Niswender CM, Jones CK, Conn PJ, Lindsley CW, Diverse effects on M1 signaling and adverse effect liability within a series of M1 ago-PAMs. ACS Chem. Nerosci 8, 866–883 (2017).

22. Kenakin T, Christopoulos A, Signalling bias in new drug discovery: Detection, quantification and therapeutic impact. Nat. Rev. Drug Discov 12, 205–216 (2013). [PubMed: 23411724]

23. Marlo JE, Niswender CM, Days EL, Bridges TM, Xiang Y, Rodriguez AL, Shirey JK, Brady AE, Nalywajko T, Luo Q, Austin CA, Williams MB, Kim K, Williams R, Orton D, Brown HA, Lindsley CW, Weaver CD, Conn PJ, Discovery and characterization of novel allosteric potentiators of M1 muscarinic receptors reveals multiple modes of activity. Mol. Pharmacol 75, 577–588 (2009). [PubMed: 19047481]

24. Brown HA, Henage LG, Preininger AM, Xiang Y, Exton JH, Biochemical analysis of phospholipase D. Methods Enzymol 434, 49–87 (2007). [PubMed: 17954242]

25. Pepitoni S, Mallon RG, Pai JK, Borkowski JA, Buck MA, McQuade RD, Phospholipase D activity and phosphatidylethanol formation in stimulated HeLa cells expressing the human m1 muscarinic acetylcholine receptor gene. Biochem. Biophys. Res. Commun 176, 453–458 (1991). [PubMed: 2018533]

26. McKenzie FR, Seuwen K, Pouysségur J, Stimulation of phosphatidylcholine breakdown by thrombin and carbachol but not by tyrosine kinase receptor ligands in cells transfected with M1 muscarinic receptors. Rapid desensitization of phosphocholine-specific (PC) phospholipase D but

sustained activity of PC-phospholipase C. J. Biol. Chem 267, 22759–22769 (1992). [PubMed: 1331066]

27. Nelson RK, Frohman MA, Physiological and pathophysiological roles for phospholipase D. J. Lipid Res 56, 2229–2237 (2015). [PubMed: 25926691]
28. Schmid CL, Kennedy NM, Ross NC, Lovell KM, Yue Z, Morgenweck J, Cameron MD, Bannister TD, Bohn LM, Bias factor and therapeutic window correlate to predict safer opioid analgesics. Cell 171, 1165–1175.e13 (2017). [PubMed: 29149605]
29. Kenakin T, Is the quest for signaling bias worth the effort? Mol. Pharmacol 93, 266–269 (2018). [PubMed: 29348268]
30. Ghoshal A, Rook JM, Dickerson JW, Roop GN, Morrison RD, Jalan-Sakrikar N, Lamsal A, Noetzel MJ, Poslusney MS, Wood MR, Melancon BJ, Stauffer SR, Xiang Z, Daniels JS, Niswender CM, Jones CK, Lindsley CW, Conn PJ, Potentiation of M_1 muscarinic receptor reverses plasticity deficits and negative and cognitive symptoms in a schizophrenia mouse model. Neuropsychopharmacology 41, 598–610 (2016). [PubMed: 26108886]
31. Ghoshal A, Moran SP, Dickerson JW, Joffe ME, Grueter BA, Xiang Z, Lindsley CW, Rook JM, Conn PJ, Role of mGlu5 receptors and inhibitory neurotransmission in M1 dependent muscarinic LTD in the prefrontal cortex: Implications in schizophrenia. ACS Chem. Nerosci 8, 2254–2265 (2017).
32. Exton JH, Regulation of phospholipase D. FEBS Lett 531, 58–61 (2002). [PubMed: 12401203]
33. Bocckino SB, Wilson PB, Exton JH, Ca^{2+}-mobilizing hormones elicit phosphatidylethanol accumulation via phospholipase D activation. FEBS Lett 225, 201–204 (1987). [PubMed: 3319693]
34. Sheffler DJ, Williams R, Bridges TM, Xiang Z, Kane AS, Byun NE, Jadhav S, Mock MM, Zheng F, Lewis LM, Jones CK, Niswender CM, Weaver CD, Lindsley CW, Conn PJ, A novel selective muscarinic acetylcholine receptor subtype 1 antagonist reduces seizures without impairing hippocampus-dependent learning. Mol. Pharmacol 76, 356–368 (2009). [PubMed: 19407080]
35. Scott SA, O'Reilly MC, Daniels JS, Morrison R, Ptak R, Dawson ES, Tower N, Engers JL, Engers DW, Oguin T, Thomas P, White L, Brown HA, Lindsley CW, in Probe Reports from the NIH Molecular Libraries Program (National Center for Biotechnology Information, 2010).
36. Lewis JA, Scott SA, Lavieri R, Buck JR, Selvy PE, Stoops SL, Armstrong MD, Brown HA, Lindsley CW, Design and synthesis of isoform-selective phospholipase D (PLD) inhibitors. Part I: Impact of alternative halogenated privileged structures for PLD1 specificity. Bioorg. Med. Chem. Lett 19, 1916–1920 (2009). [PubMed: 19268584]
37. Lavieri R, Scott SA, Lewis JA, Selvy PE, Armstrong MD, Alex Brown H, Lindsley CW, Design and synthesis of isoform-selective phospholipase D (PLD) inhibitors. Part II. Identification of the 1,3,8-triazaspiro[4,5]decan-4-one privileged structure that engenders PLD2 selectivity. Bioorg. Med. Chem. Lett 19, 2240–2243 (2009). [PubMed: 19299128]
38. Reid PR, Bridges TM, Sheffler DJ, Cho HP, Lewis LM, Days E, Daniels JS, Jones CK, Niswender CM, Weaver CD, Conn PJ, Lindsley CW, Wood MR, Discovery and optimization of a novel, selective and brain penetrant M1 positive allosteric modulator (PAM): The development of ML169, an MLPCN probe. Bioorg. Med. Chem. Lett 21, 2697–2701 (2011). [PubMed: 21194936]
39. Martin HGS, Bernabeu A, Lassalle O, Bouille C, Beurrier C, Pelissier-Alicot A-L, Manzoni OJ, Endocannabinoids mediate muscarinic acetylcholine receptor-dependent long-term depression in the adult medial prefrontal cortex. Front. Cell. Neurosci 9, 457 (2015). [PubMed: 26648844]
40. Walker AG, Wenthur CJ, Xiang Z, Rook JM, Emmitte KA, Niswender CM, Lindsley CW, Conn PJ, Metabotropic glutamate receptor 3 activation is required for long-term depression in medial prefrontal cortex and fear extinction. Proc. Natl. Acad. Sci. U.S.A 112, 1196–1201 (2015). [PubMed: 25583490]
41. Joffe ME, Santiago CI, Engers JL, Lindsley CW, Conn PJ, Metabotropic glutamate receptor subtype 3 gates acute stress-induced dysregulation of amygdalo-cortical function. Mol. Psychiatry 24, 916–927 (2017). [PubMed: 29269844]
42. Joffe ME, Santiago CI, Stansley BJ, Maksymetz J, Gogliotti RG, Engers JL, Nicoletti F, Lindsley CW, Conn PJ, Mechanisms underlying prelimbic prefrontal cortex mGlu3/mGlu5-dependent

plasticity and reversal learning deficits following acute stress. Neuropharmacology 144, 19–28 (2019). [PubMed: 30326237]

43. Lane JR, May LT, Parton RG, Sexton PM, Christopoulos A, A kinetic view of GPCR allostery and biased agonism. Nat. Chem. Biol 13, 929–937 (2017). [PubMed: 28820879]
44. Wootten D, Christopoulos A, Marti-Solano M, Babu MM, Sexton PM, Mechanisms of signalling and biased agonism in G protein-coupled receptors. Nat. Rev. Mol. Cell Biol 19, 638–653 (2018). [PubMed: 30104700]
45. Conn PJ, Christopoulos A, Lindsley CW, Allosteric modulators of GPCRs: A novel approach for the treatment of CNS disorders. Nat. Rev. Drug Discov 8, 41–54 (2009). [PubMed: 19116626]
46. Kenakin TP, Biased signalling and allosteric machines: New vistas and challenges for drug discovery. Br. J. Pharmacol 165, 1659–1669 (2012). [PubMed: 22023017]
47. Davoren JE, Garnsey M, Pettersen B, Brodney MA, Edgerton JR, Fortin J-P, Grimwood S, Harris AR, Jenkinson S, Kenakin T, Lazzaro JT, Lee C-W, Lotarski SM, Nottebaum L, O'Neil SV, Popiolek M, Ramsey S, Steyn SJ, Thorn CA, Zhang L, Webb D, Design and synthesis of γ- and δ-lactam M1 positive allosteric modulators (PAMs): Convulsion and cholinergic toxicity of an M1-selective PAM with weak agonist activity. J. Med. Chem 60, 6649–6663 (2017). [PubMed: 28598634]
48. Lv X, Dickerson JW, Rook JM, Lindsley CW, Conn PJ, Xiang Z, M1 muscarinic activation induces long-lasting increase in intrinsic excitability of striatal projection neurons. Neuropharmacology 118, 209–222 (2017). [PubMed: 28336323]
49. Xiang Z, Thompson AD, Jones CK, Lindsley CW, Conn PJ, Roles of the M1 muscarinic acetylcholine receptor subtype in the regulation of basal ganglia function and implications for the treatment of Parkinson's disease. J. Pharmacol. Exp. Ther 340, 595–603 (2012). [PubMed: 22135383]
50. Bymaster FP, Whitesitt CA, Shannon HE, DeLapp N, Ward JS, Calligaro DO, Shipley LA, Buelke-Sam JL, Bodick NC, Farde L, Sheardown MJ, Olesen PH, Hansen KT, Suzdak PD, Swedberg MDB, Sauerberg P, Mitch CH, Xanomeline: A selective muscarinic agonist for the treatment of Alzheimer's disease. Drug Dev. Res 40, 158–170 (1997).
51. Hall H, Iulita MF, Gubert P, Flores Aguilar L, Ducatenzeiler A, Fisher A, Cuello AC, AF710B, an M1/sigma-1 receptor agonist with long-lasting disease-modifying properties in a transgenic rat model of Alzheimer's disease. Alzheimers Dement 14, 811–823 (2018). [PubMed: 29291374]
52. Ma L, Seager MA, Wittmann M, Jacobson M, Bickel D, Burno M, Jones K, Graufelds VK, Xu G, Pearson M, McCampbell A, Gaspar R, Shughrue P, Danziger A, Regan C, Flick R, Pascarella D, Garson S, Doran S, Kreatsoulas C, Veng L, Lindsley CW, Shipe W, Kuduk S, Sur C, Kinney G, Seabrook GR, Ray WJ, Selective activation of the M_1 muscarinic acetylcholine receptor achieved by allosteric potentiation. Proc. Natl. Acad. Sci. U.S.A 106, 15950–15955 (2009). [PubMed: 19717450]
53. Gould RW, Dencker D, Grannan M, Bubser M, Zhan X, Wess J, Xiang Z, Locuson C, Lindsley CW, Conn PJ, Jones CK, Role for the M1 muscarinic acetylcholine receptor in top-down cognitive processing using a touchscreen visual discrimination task in mice. ACS Chem. Nerosci 6, 1683–1695 (2015).
54. Vardigan JD, Cannon CE, Puri V, Dancho M, Koser A, Wittmann M, Kuduk SD, Renger JJ, Uslaner JM, Improved cognition without adverse effects: Novel M1 muscarinic potentiator compares favorably to donepezil and xanomeline in rhesus monkey. Psychopharmacology 232, 1859–1866 (2015). [PubMed: 25491927]
55. Davoren JE, O'Neil SV, Anderson DP, Brodney MA, Chenard L, Dlugolenski K, Edgerton JR, Green M, Garnsey M, Grimwood S, Harris AR, Kauffman GW, LaChapelle E, Lazzaro JT, Lee C-W, Lotarski SM, Nason DM, Obach RS, Reinhart V, Salomon-Ferrer R, Steyn SJ, Webb D, Yan J, Zhang L, Design and optimization of selective azaindole amide M1 positive allosteric modulators. Bioorg. Med. Chem. Lett 26, 650–655 (2016). [PubMed: 26631313]
56. Digby GJ, Noetzel MJ, Bubser M, Utley TJ, Walker AG, Byun NE, Lebois EP, Xiang Z, Sheffler DJ, Cho HP, Davis AA, Nemirovsky NE, Mennenga SE, Camp BW, Bimonte-Nelson HA, Bode J, Italiano K, Morrison R, Daniels JS, Niswender CM, Olive MF, Lindsley CW, Jones CK, Conn PJ, Novel allosteric agonists of M_1 muscarinic acetylcholine receptors induce brain region-specific

responses that correspond with behavioral effects in animal models. J. Neurosci 32, 8532–8544 (2012). [PubMed: 22723693]

57. Lebois EP, Schroeder JP, Esparza TJ, Bridges TM, Lindsley CW, Conn PJ, Brody DL, Daniels JS, Levey AI, Disease-modifying effects of M1 muscarinic acetylcholine receptor activation in an Alzheimer's disease mouse model. ACS Chem. Nerosci 8, 1177–1187 (2017).
58. Kurimoto E, Matsuda S, Shimizu Y, Sako Y, Mandai T, Sugimoto T, Sakamoto H, Kimura H, An approach to discovering novel muscarinic M1 receptor positive allosteric modulators with potent cognitive improvement and minimized gastrointestinal dysfunction. J. Pharmacol. Exp. Ther 364, 28–37 (2018). [PubMed: 29025977]
59. Walker SJ, Brown HA, Measurement of G protein-coupled receptor-stimulated phospholipase D activity in intact cells. Methods Mol. Biol 237, 89–97 (2004). [PubMed: 14501041]
60. Ghoshal A, Conn PJ, The hippocampo-prefrontal pathway: A possible therapeutic target for negative and cognitive symptoms of schizophrenia. Future Neurol 10, 115–128 (2015). [PubMed: 25825588]
61. Maksymetz J, Joffe ME, Moran SP, Stansley BJ, Li B, Temple K, Engers DW, Lawrence JJ, Lindsley CW, Conn PJ, M_1 muscarinic receptors modulate fear-related inputs to the prefrontal cortex: Implications for novel treatments of posttraumatic stress disorder. Biol. Psychiatry 85, 989–1000 (2019). [PubMed: 31003787]
62. Scarr E, Sundram S, Keriakous D, Dean B, Altered hippocampal muscarinic M4, but not M1, receptor expression from subjects with schizophrenia. Biol. Psychiatry 61, 1161–1170 (2007). [PubMed: 17239354]
63. Dean B, Hopper S, Conn PJ, Scarr E, Changes in BQCA allosteric modulation of [^{3}H]NMS binding to human cortex within schizophrenia and by divalent cations. Neuropsychopharmacology 41, 1620–1628 (2016). [PubMed: 26511338]
64. Dean B, McLeod M, Keriakous D, McKenzie J, Scarr E, Decreased muscarinic1 receptors in the dorsolateral prefrontal cortex of subjects with schizophrenia. Mol. Psychiatry 7, 1083–1091 (2002). [PubMed: 12476323]
65. Scarr E, Udawela M, Thomas EA, Dean B, Changed gene expression in subjects with schizophrenia and low cortical muscarinic M1 receptors predicts disrupted upstream pathways interacting with that receptor. Mol. Psychiatry 23, 295–303 (2018). [PubMed: 27801890]
66. Scarr E, Cowie TF, Kanellakis S, Sundram S, Pantelis C, Dean B, Decreased cortical muscarinic receptors define a subgroup of subjects with schizophrenia. Mol. Psychiatry 14, 1017–1023 (2009). [PubMed: 18317461]
67. Caccamo A, Oddo S, Billings LM, Green KN, Martinez-Coria H, Fisher A, LaFerla FM, M1 receptors play a central role in modulating AD-like pathology in transgenic mice. Neuron 49, 671–682 (2006). [PubMed: 16504943]
68. Medeiros R, Kitazawa M, Caccamo A, Baglietto-Vargas D, Estrada-Hernandez T, Cribbs DH, Fisher A, LaFerla FM, Loss of muscarinic M_1 receptor exacerbates Alzheimer's disease-like pathology and cognitive decline. Am. J. Pathol 179, 980–991 (2011). [PubMed: 21704011]
69. Rook JM, Xiang Z, Lv X, Ghoshal A, Dickerson JW, Bridges TM, Johnson KA, Foster DJ, Gregory KJ, Vinson PN, Thompson AD, Byun N, Collier RL, Bubser M, Nedelcovych MT, Gould RW, Stauffer SR, Daniels JS, Niswender CM, Lavreysen H, Mackie C, Conde-Ceide S, Alcazar J, Bartolomé-Nebreda JM, Macdonald GJ, Talpos JC, Steckler T, Jones CK, Lindsley CW, Conn PJ, Biased mGlu5-positive allosteric modulators provide in vivo efficacy without potentiating mGlu5 modulation of NMDAR currents. Neuron 86, 1029–1040 (2015). [PubMed: 25937172]
70. Parmentier-Batteur S, Hutson PH, Menzel K, Uslaner JM, Mattson BA, O'Brien JA, Magliaro BC, Forest T, Stump CA, Tynebor RM, Anthony NJ, Tucker TJ, Zhang X-F, Gomez R, Huszar SL, Lambeng N, Fauré H, Le Poul E, Poli S, Rosahl TW, Rocher J-P, Hargreaves R, Williams TM, Mechanism based neurotoxicity of mGlu5 positive allosteric modulators—Development challenges for a promising novel antipsychotic target. Neuropharmacology 82, 161–173 (2014). [PubMed: 23291536]
71. O'Brien DE, Shaw DM, Cho HP, Cross AJ, Wesolowski SS, Felts AS, Bergare J, Elmore CS, Lindsley CW, Niswender CM, Conn PJ, Differential pharmacology and binding of mGlu2 receptor allosteric modulators. Mol. Pharmacol 93, 526–540 (2018). [PubMed: 29545267]

72. Hammond AS, Rodriguez AL, Townsend SD, Niswender CM, Gregory KJ, Lindsley CW, Conn PJ, Discovery of a novel chemical class of mGlu5 allosteric ligands with distinct modes of pharmacology. ACS Chem. Nerosci 1, 702–716 (2010).

73. Rodriguez AL, Tarr JC, Zhou Y, Williams R, Gregory KJ, Bridges TM, Daniels JS, Niswender CM, Conn PJ, Lindsley CW, Stauffer SR, in Probe Reports from the NIH Molecular Libraries Program (National Center for Biotechnology Information, 2010).

74. Khajehali E, Valant C, Jörg M, Tobin AB, Conn PJ, Lindsley CW, Sexton PM, Scammells PJ, Christopoulos A, Probing the binding site of novel selective positive allosteric modulators at the M_1 muscarinic acetylcholine receptor. Biochem. Pharmacol 154, 243–254 (2018). [PubMed: 29777683]

75. Thal DM, Sun B, Feng D, Nawaratne V, Leach K, Felder CC, Bures MG, Evans DA, Weis WI, Bachhawat P, Kobilka TS, Sexton PM, Kobilka BK, Christopoulos A, Crystal structures of the M1 and M4 muscarinic acetylcholine receptors. Nature 531, 335–340 (2016). [PubMed: 26958838]

76. Lein ES, Hawrylycz MJ, Ao N, Ayres M, Bensinger A, Bernard A, Boe AF, Boguski MS, Brockway KS, Byrnes EJ, Chen L, Chen L, Chen T-M, Chin MC, Chong J, Crook BE, Czaplinska A, Dang CN, Datta S, Dee NR, Desaki AL, Desta T, Diep E, Dolbeare TA, Donelan MJ, Dong H-W, Dougherty JG, Duncan BJ, Ebbert AJ, Eichele G, Estin LK, Faber C, Facer BA, Fields R, Fischer SR, Fliss TP, Frensley C, Gates SN, Glattfelder KJ, Halverson KR, Hart MR, Hohmann JG, Howell MP, Jeung DP, Johnson RA, Karr PT, Kawal R, Kidney JM, Knapik RH, Kuan CL, Lake JH, Laramee AR, Larsen KD, Lau C, Lemon TA, Liang AJ, Liu Y, Luong LT, Michaels J, Morgan JJ, Morgan RJ, Mortrud MT, Mosqueda NF, Ng LL, Ng R, Orta GJ, Overly CC, Pak TH, Parry SE, Pathak SD, Pearson OC, Puchalski RB, Riley ZL, Rockett HR, Rowland SA, Royall JJ, Ruiz MJ, Sarno NR, Schaffnit K, Shapovalova NV, Sivisay T, Slaughterbeck CR, Smith SC, Smith KA, Smith BI, Sodt AJ, Stewart NN, Stumpf K-R, Sunkin SM, Sutram M, Tam A, Teemer CD, Thaller C, Thompson CL, Varnam LR, Visel A, Whitlock RM, Wohnoutka PE, Wolkey CK, Wong VY, Wood M, Yaylaoglu MB, Young RC, Youngstrom BL, Yuan XF, Zhang B, Zwingman TA, Jones AR, Genome-wide atlas of gene expression in the adult mouse brain. Nature 445, 168–176 (2007). [PubMed: 17151600]

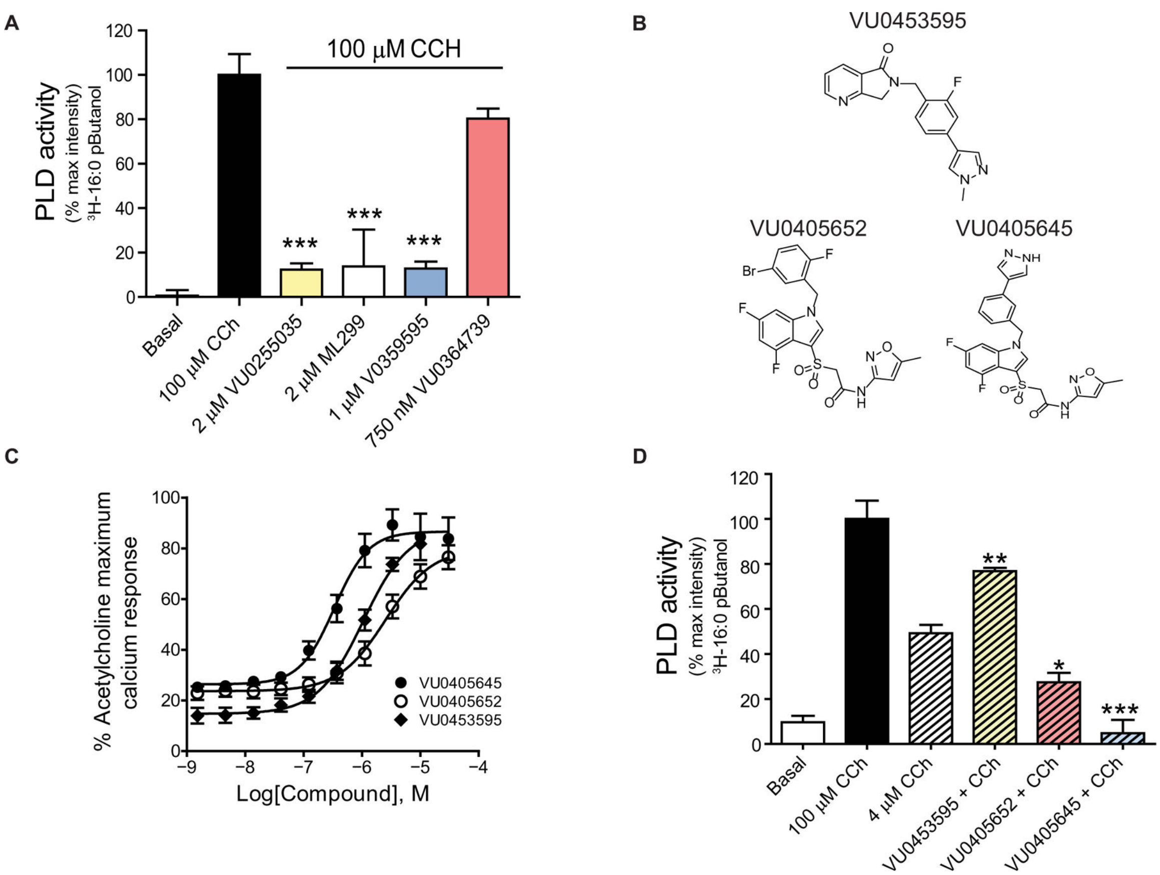

Fig. 1. M_1 receptor activation leads to PLD activity in hM_1-CHO cells, and M_1 PAMs show differential signal bias in potentiating M_1-mediated PLD signaling.

(**A**) rM_1-CHO cells were treated with DMSO (basal) or 100 μM CCh alone or in combination with 2 μM VU0255035 (M_1 antagonist), 2 μM ML299 ($PLD_{1,2}$ inhibitor), 1 μM VU0359595 (PLD_1 inhibitor), or 750 nM VU0364739 (PLD_2 inhibitor). PLD activity was measured by quantification of the PLD product pButanol. The extent of PLD activity in response to 100 μM CCh alone was set at 100%. The effects of the M_1 receptor antagonist or various pharmacological inhibitors of PLD were compared to the maximal effect elicited by 100 μM CCh (one-way ANOVA $F_{4,10} = 29.34$; $P = 0.0001$, with post hoc Dunnett's test using 100 μM CCh alone as the control group, ***$P < 0.001$). (**B**) Structures of the M_1 receptor PAMs VU0453595, VU0405652, and VU0405645. (**C**) rM_1-CHO cells were treated with an EC_{20} concentration of ACh in the presence of the indicated concentrations of VU0453595, VU0405652, and VU0405645 and then were assayed for Ca^{2+} signaling with the Functional Drug Screening System (FDSS7000). (**D**) Using rM_1-CHO cells under the same conditions described earlier, the extent of PLD activation relative to a maximal response of 100 μM CCh alone was evaluated for 4 μM CCh in the presence of DMSO, 10 μM VU0453595, 10 μM VU0405652, or 10 μM VU0405645 (one-way ANOVA $F_{3,8} = 55.1$; $P = 0.0001$, with post hoc Dunnett's test using 4 μM CCh; *$P < 0.05$, **$P < 0.01$, and ***$P < 0.001$). Data in (A), (C), and (D) are means ± SEM from three independent experiments each performed in triplicate.

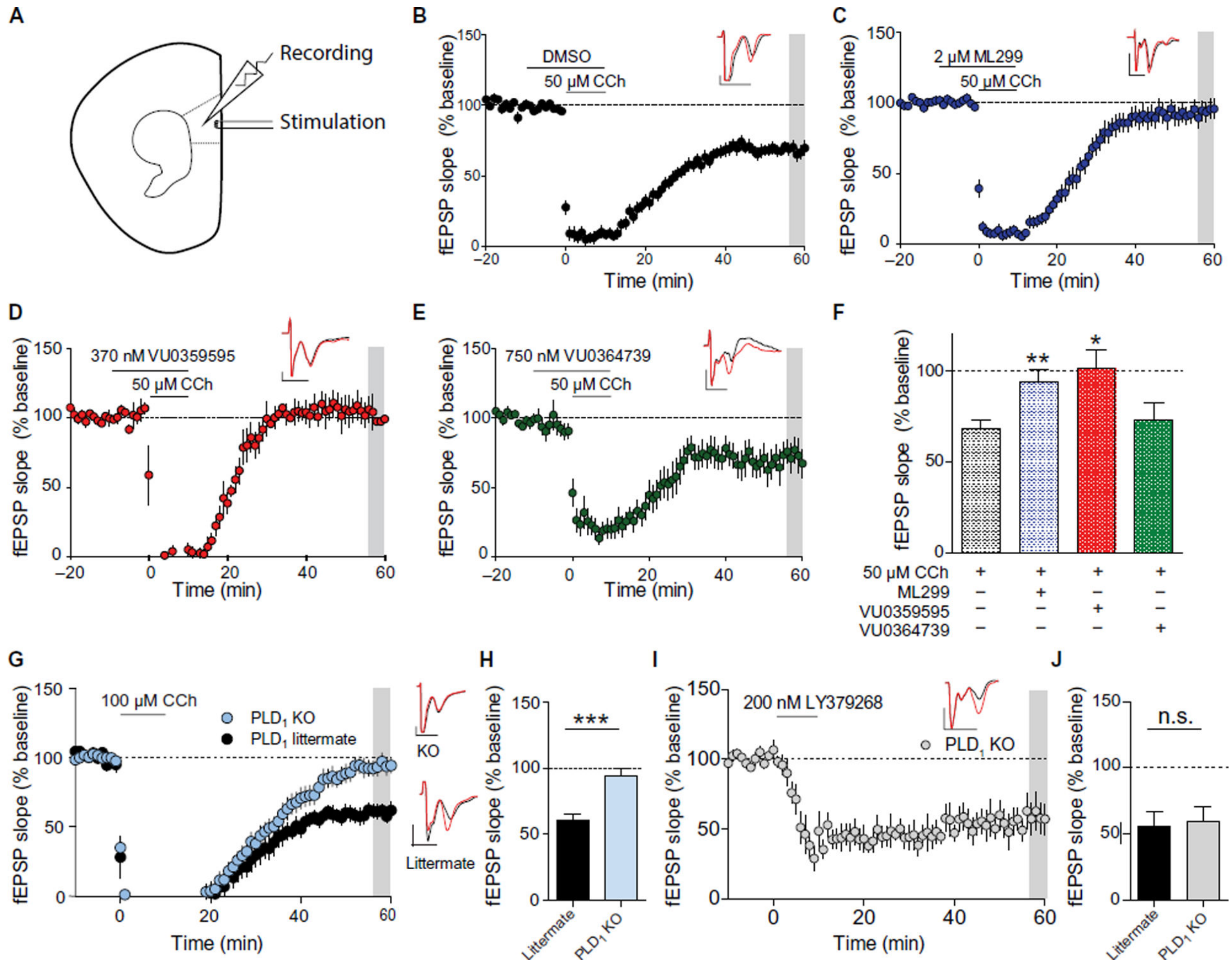

Fig. 2. PLD_1, but not PLD_2, is necessary for CCh-dependent LTD in the mPFC.

(**A**) Schematic of the field excitatory postsynaptic potentials (fEPSPs) recorded from layer V of the mouse mPFC in response to electrical stimulation in the superficial layers II to III. (**B**) Time course graph for fEPSP slope normalized to the average baseline. Carbachol (CCh) (50 μM) induced a long-term depression (LTD) of fEPSP slope [68.0 ± 4.44%, n/N = 26/20 (n = number of slices/N = number of mice)]. (**C**) Time course graph for fEPSP slope with a 10-min pretreatment with the $PLD_{1,2}$ inhibitor ML299 (2 μM) followed by a 10-min co-application of ML299 and 50 μM CCh (93.8 ± 6.74%, n/N = 21/10). (**D**) Time course graph for fEPSP slope normalized to baseline with a 10-min pretreatment with the PLD_1-specific inhibitor VU0359595 (370 nM) and 10-min co-application of 50 μM CCh (101 ± 10.1%, n/N = 7/6). (**E**) Time course graph for fEPSP slope normalized to baseline with a 10-min pretreatment with the PLD_2-selective inhibitor VU0364739 (750 nM) and 10-min co-application of 50 μM CCh (69.3 ± 13.0, n/N = 8/4). Insets in (B) to (E) show representative fEPSP traces for each condition for baseline (red trace) and 50 min after CCh washout (black trace). (**F**) Quantification of the average fEPSP slope 46 to 50 min after drug washout [shaded areas in (B) to (E)] (one-way ANOVA $F_{3,58}$ = 5.21; P = 0.0029, with post hoc Dunnett's test using 50 μM CCh alone as the control group; *P < 0.05 and **P < 0.01). (**G**) Left: Time course graph of fEPSP slope normalized to baseline with bath application of CCh

(100 μM) in littermate controls (59.6 ± 6.06 *n*/*N* = 9/6) and PLD1 KO mice (92.2 ± 3.21, *n*/*N* = 9/6). Right: Representative fEPSP traces for baseline (red trace) and 50 min after CCh washout (black trace) for PLD_1 KO animals (top) and littermate controls (bottom). (**H**) Quantification of the average fEPSP slope 46 to 50 min after drug washout [shaded area in (G)] (Student's *t* test; $P = 0.0002$; ****P* < 0.001). (**I**) Time course graph for fEPSP slope normalized to baseline with 10-min bath application of the group II metabotropic glutamate receptor agonist LY379268 (200 nM) in PLD_1 KO mice (59.4 ± 11.4%, *n*/*N* = 5/3). (**J**) Quantification of the average fEPSP slope 46 to 50 min after LY379268 (200 nM) washout [shaded area in (I)] for PLD_1 KO mice and littermate controls (55.7 ± 11.6%, *n*/*N* = 7/3; Student's *t* test; $P = 0.828$). Inset shows representative fEPSP traces for each condition for baseline (red trace) and 50 min after LY379268 washout (black trace). Scale bars, 0.25 mV (*y* axis) and 5 ms (*x* axis). Data are means ± SEM. n.s., not significant.

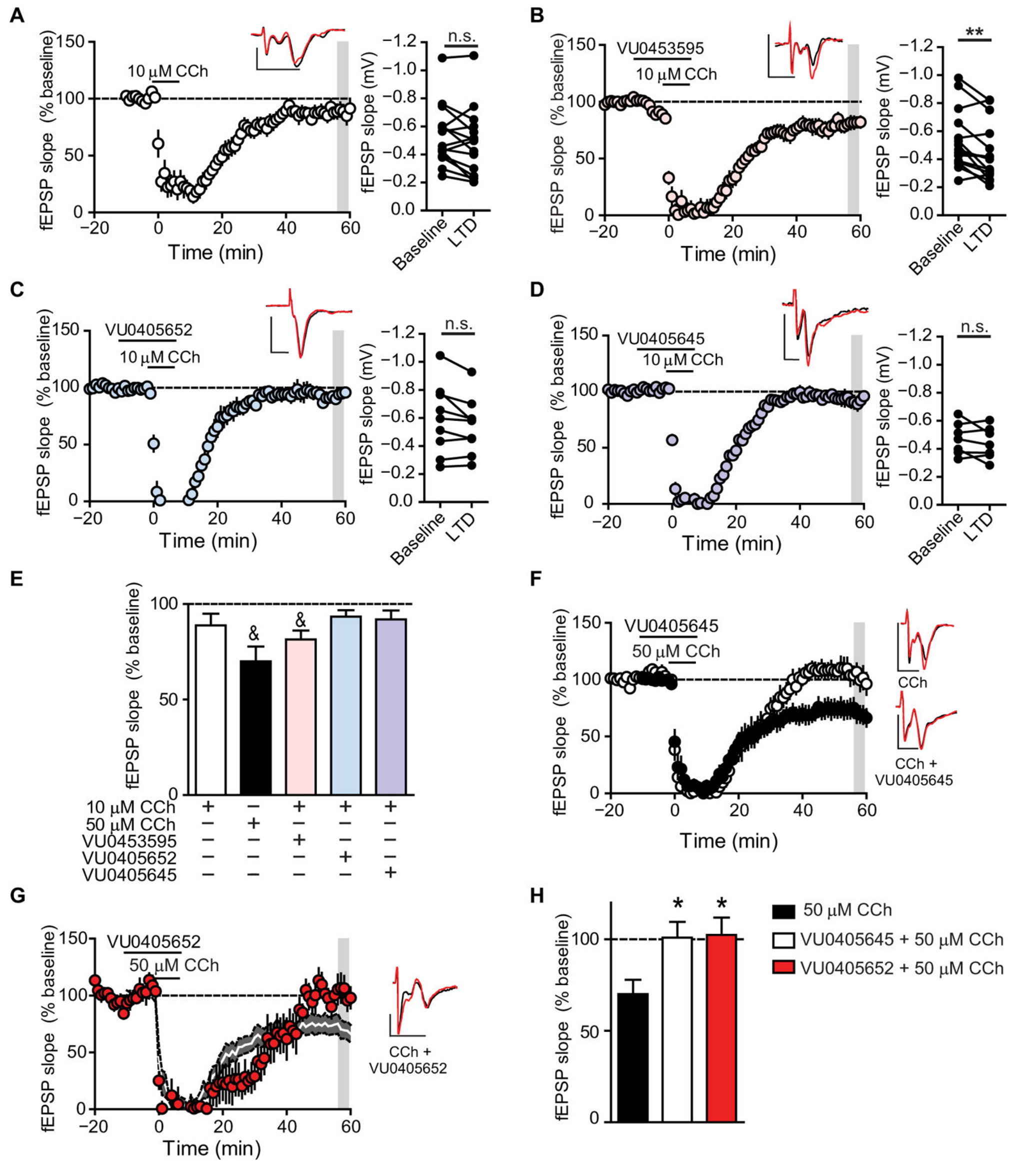

Fig. 3. Biased M_1 PAMs fail to potentiate a submaximal mLTD in the mPFC and actively block CCh-dependent LTD.

(**A**) Left: Time course graph for fEPSP slope normalized to the average baseline. Right: Comparison of fEPSP slope during baseline and 46 to 50 min after CCh (10 μM) washout (shaded area). A 10-min bath application of CCh (10 μM) induced a minimal LTD of fEPSP slope (88.9 ± 6.05, *n*/*N* = 15/13; paired *t* test; *P* > 0.05). (**B**) A 10-min pretreatment with the nonbiased M_1 PAM VU0453595 (10 M) followed by a 10-min co-application of VU0453595 + CCh (10 μM) (81.5 ± 4.70%, *n*/*N* = 14/11; paired *t* test; *P* = 0.01). (**C**) A 10-min pretreatment with the biased M_1 PAM VU0405652 (10 μM) followed by a 10-min co-application of VU0405652 + 10 μM CCh (93.5 ± 3.28%, *n*/*N* = 9/8; paired *t* test; *P* > 0.05). (**D**) A 10-min pretreatment with the biased M_1 PAM VU0405645 (10 μM) followed by a 10-min co-application of VU0405645 + CCh (10 μM) (91.9 ± 4.67%, *n*/*N* = 7/7; paired *t* test; *P* > 0.05). Insets contain representative fEPSP traces for each condition for baseline (red trace) and 50 min after CCh washout (black trace). Scale bars, 0.5 mV and 5 ms. Data are means ±

SEM. **$P \leq 0.01$. (**E**) Summary of the last 5 min of the recordings from the time course experiments ($^{\&}P < 0.05$, paired *t* test). (**F**) Left: Time course graph for fEPSP slope normalized to the average baseline. CCh (50 μM, black) (70.0 ± 7.78%, $n/N = 9/7$) alone compared to a 10-min pretreatment with VU0405645 (10 μM) and a 10-min co-application of CCh (50 μM, white) (101 ± 8.59%, $n/N = 11/8$). Right: Representative fEPSP traces for each condition for baseline (red trace) and 50 min after CCh washout (black trace). Scale bars, 0.5 mV and 5 ms. (**G**) Time course graph of normalized fEPSP slope of a 10-min pretreatment with VU0405652 (75 μM) and 10-min application of CCh (50 μM, red) (102 ± 9.46%, $n/N = 7/3$) compared to CCh alone [shaded time course corresponds to CCh (50 μM) from (F); the solid white line represents the mean fEPSP slope, and the gray shaded region around the line shows ±SEM]. (**H**) Quantification of the average fEPSP slope 46 to 50 min after CCh washout (shaded area) (one-way ANOVA $F_{3,25} = 4.554$; $P = 0.0216$, with post hoc Dunnett's test using CCh alone as the control group; *$P < 0.05$).

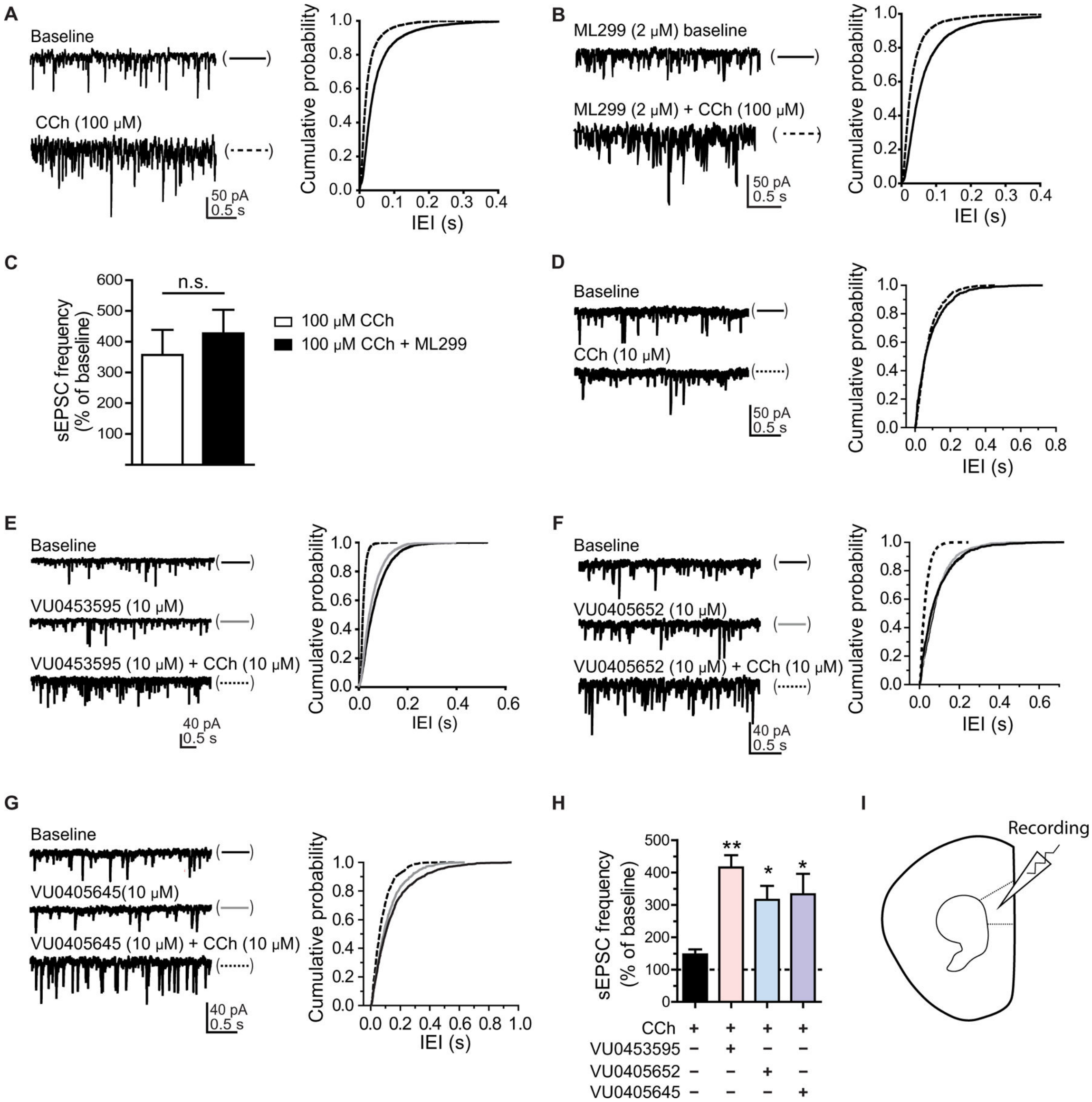

Fig. 4. PLD is not required for the M_1-dependent increase in sEPSC frequency in mPFC layer V pyramidal neurons, and both biased and nonbiased M_1 PAMs potentiate this response.

(**A**) Sample traces (left) and the cumulative probability of interevent interval (IEI) (right) of sEPSCs during baseline and during application of CCh (100 μM) as indicated for a typical cell. (**B**) Sample traces (left) and the IEI cumulative probability (right) of sEPSCs in baseline with the $PLD_{1,2}$ inhibitor ML299 (2 μM) and during application of a combination of ML299 and CCh (100 μM) for a typical cell. (**C**) Quantification of the average increase in sEPSC frequency between treatment with CCh alone [357.0 ± 81.6%, n/N = 7/3 (n = number of cells/N = number of animals)] and CCh in the presence of ML299 (427.0 ± 76.5%, n/N = 8/3) (Student's t test; $P > 0.05$). (**D**) Sample traces (left) and IEI cumulative probability (right) of sEPSCs in baseline and during application of CCh (10 μM) from a typical cell. (**E** to **G**) Sample traces (left) and IEI cumulative probability (right) of sEPSCs in baseline, during application of the indicated PAM, and during treatment with a PAM and CCh as indicated for typical cells. (**H**) Quantification of the peak effect on sEPSC frequency for

CCh (10 μM) alone (147 ± 15.4%, *n*/*N* = 7/3), CCh with VU0453595 (10 μM) (416 ± 38.2%, *n*/*N* = 8/4), CCh with VU0405652 (10 μM) (316 ± 43.3%, *n*/*N* = 10/5), and CCh with VU0405645 (10 μM) (332.4 ± 63.7%, *n*/*N* = 11/4). One-way ANOVA $F_{3,35} = 5.77$; $P = 0.0026$, with post hoc Dunnett's test using CCh alone as the control group; *$P < 0.05$ and **$P < 0.01$. Data are means ± SEM. (**I**) Schematic of whole-cell recordings from mPFC layer V pyramidal neurons (regular spiking cells) clamped at −70 mV.

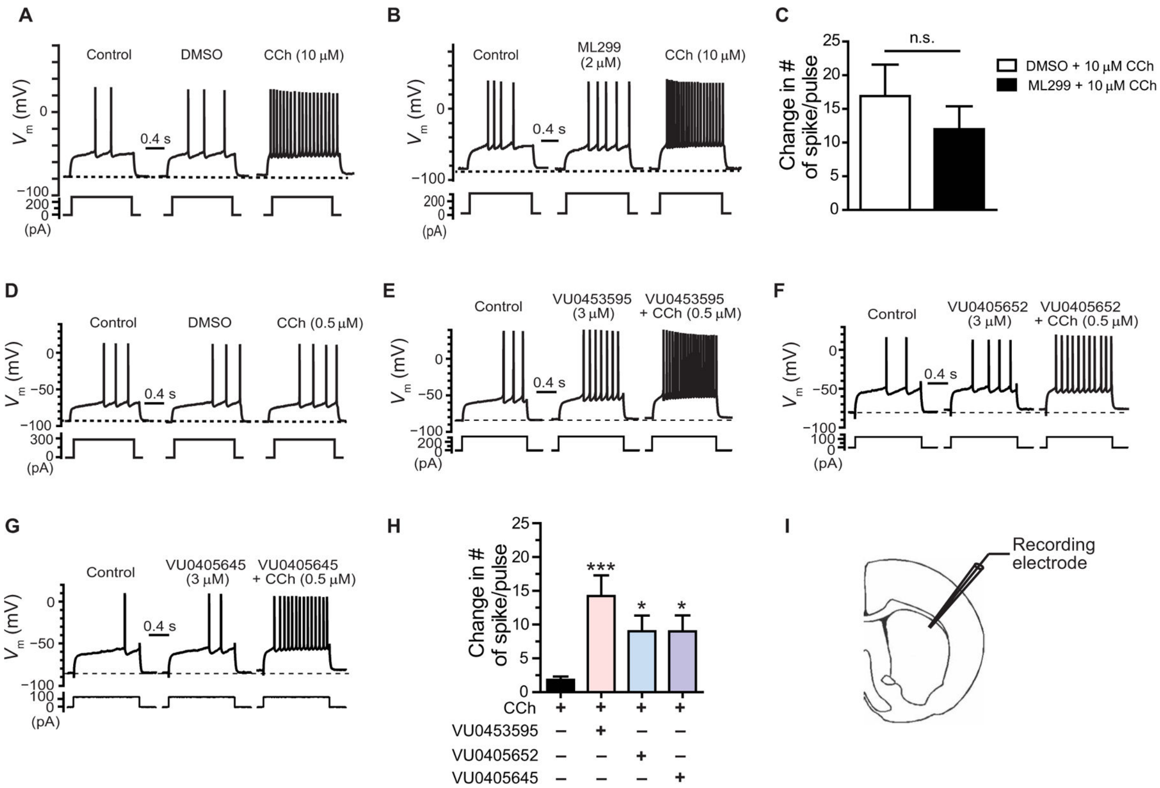

Fig. 5. PLD is not necessary for M_1-dependent effects on the excitability of striatal SPNs, and both biased and nonbiased M_1 PAMs potentiate this response.

(**A**) Sample traces of membrane potential responses to a depolarization current step from an SPN during baseline and in the presence of DMSO and CCh (10 μM). (**B**) Effect of pretreatment with ML299 (2 μM) and then co-application of CCh (10 μM) on SPN excitability. (**C**) Bar graph summarizing the changes in the number of spikes per pulse after CCh (10 μM) application in the presence of ML299 (12.0 ± 3.38, *n*/*N* = 6/5) or DMSO (16.9 ± 4.67, *n*/*N* = 5/5) showed no statistically significant difference between groups (Student's *t* test; $P > 0.05$). (**D** to **G**) Sample traces of membrane potential responses to a depolarization current step from an SPN during baseline, in the presence of the indicated M_1 PAM (3 μM) or DMSO, and then M_1 PAM/DMSO + CCh (0.5 μM). (**H**) Bar graph summarizing the changes in the number of spikes per pulse after CCh (0.5 μM) application in the presence of DMSO (1.83 ± 0.49, *n*/*N* = 9/7), VU0453595 (14.2 ± 3.05, *n*/*N* = 6/6), VU0405652 (9.02 ± 2.31, *n*/*N* = 7/6), and VU0405645 (9.00 ± 2.37, *n*/*N* = 6/5) (one-way ANOVA $F_{3,24} = 6$; $P = 0.0017$, with post hoc Dunnett's test using CCh + DMSO as the control group; *$P < 0.05$ and ***$P < 0.001$). Data are means ± SEM. (**I**) Schematic of whole-cell recordings from SPN neurons under current clamp conditions performed in the dorsal lateral striatum (DLS).